Supporting Information

Control covered compositions and morphologies of uranium oxide nanocrystals in solution phase: multi-monomer growth and self-catalysis

Qiang Yan[ab], Yiwu Mao[a], Xiaosong Zhou[a], Jianhua Liang[a], Shuming Peng[a*], Minyou Ye[b*]

[a]Institute of Nuclear Physics and Chemistry, China Academy of Engineering Physics, Mianyang, Sichuan, 621900, China
[b]School of Physical Sciences, University of Science and Technology of China, Hefei, 230026, China

*corresponding authors:
Email addresses: pengshuming@caep.cn(S.M. Peng),
yemy@ustc.edu.cn (M.Y. Ye)

Section 1: Compositions and morphologies control

Figure S1. XRD patterns (a) of products obtained at different pH values (UO_2: pH=9.81 red; U_4O_9: pH=10.66, blue. Symbols:● = U_4O_9;◆= UO_2) and XPS spectroscopy (b and c) of stoichiometric uranium oxide.

Table S1. The products at different pH values (T = 200°C, t = 6 hours).

Figure S2. SEM images of products from the experiments described in Table S1. Products: a, $UO_3 \cdot H_2O$; b, $UO_3 \cdot H_2O$ (major) and U_3O_8; c, U_3O_8; d, U_3O_8 (rod) and UO_2 (particle); e, UO_2; f, U_4O_9.

Table S2.1. The experimental parameters for U_3O_8 morphological control.

Table S2.2. The experimental parameters for UO_2 morphological control.

Figure S3. XRD patterns of various morphologies U_3O_8 (a) and UO_2 (b).

Section 2: multi-monomer growth mechanisms and verified experiments

Table S3.1. The experimental parameters to control compositions (UAH = 200 mg, DI water = 5 mL, acetone = 10mL, T = 200 °C, t = 6 h).

Section 3: Self-catalytic mechanisms and verified experiments

Section 1. Compositions and morphologies control

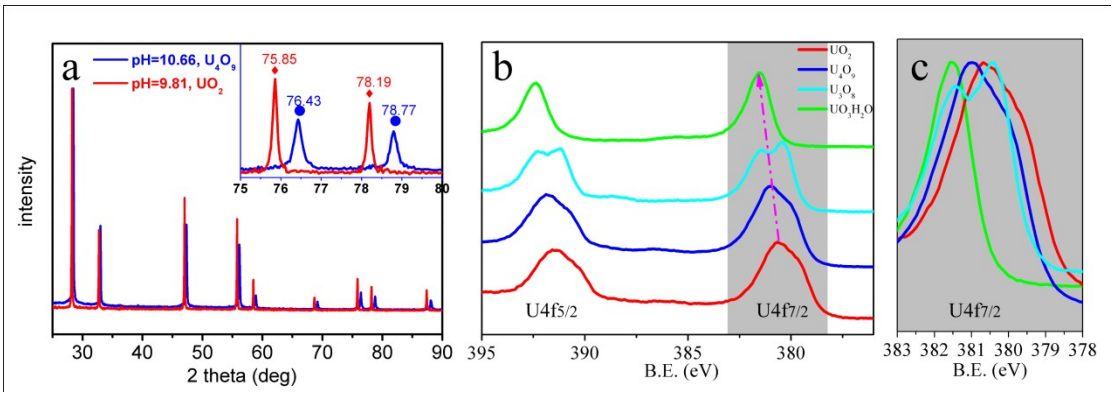

Figure S1. XRD patterns (a) of products obtained at different pH values (UO_2: pH=9.81 red curve; U_4O_9: pH=10.66, blue curve. Symbols:● = U_4O_9;◆= UO_2) and XPS spectroscopy (b and c) of stoichiometric uranium oxide.

The U_4O_9 (a/4 = 5.43 Å) lattice parameter is slightly smaller than UO_2 (a = 5.46 Å), which results in a larger 2 theta for each correspond peak. The average valence state of $U(V+VI)_4O_9$ (b and c, blue curve) is higher than the valance state of U (VI) O_2 (b and c, red curve), which results in a higher binding energy of U_{4f}. Peak positions of binding energy shift to higher from UO_2, U_4O_9, U_3O_8 to $UO_3{\cdot}H_2O$.

Table S1. The products at different pH values (T = 200°C, t = 6 hours).

Sample ID	DI water mL	Acetone mL	UAH mg	$NH_3{\cdot}H_2O$ μL	pH	Products
S1-a	**15**	**-**	**100**	**50**	**-**	**$UO_3{\cdot}H_2O$**
S1-b	5	10	100	**25**	**4.76**	$UO_3{\cdot}H_2O$ & U_3O_8
S1-c	5	10	100	**75**	**7.83**	U_3O_8
S1-d	5	10	100	**100**	**8.25**	U_3O_8 & UO_2
S1-e	5	10	100	**300**	**9.81**	UO_2
S1-f	5	10	100	**1500**	**10.66**	U_4O_9

The oxidation state of uranium in the final products decreased from the U(VI) $O_3{\cdot}H_2O$ and $U(VI+V)_3O_8$ to $U(IV)O_2$ with an increasing pH value (from 4.67 to 9.81). This implies that the reducing ability of system increases with increasing pH values. The appearance of the $U(V+IV)_4O_9$ at higher pH values (10.66) is due to a high particle concentration in solution, shortened the monomer diffusion distance and induced rapid U(V) growth packaging into nanoparticles.

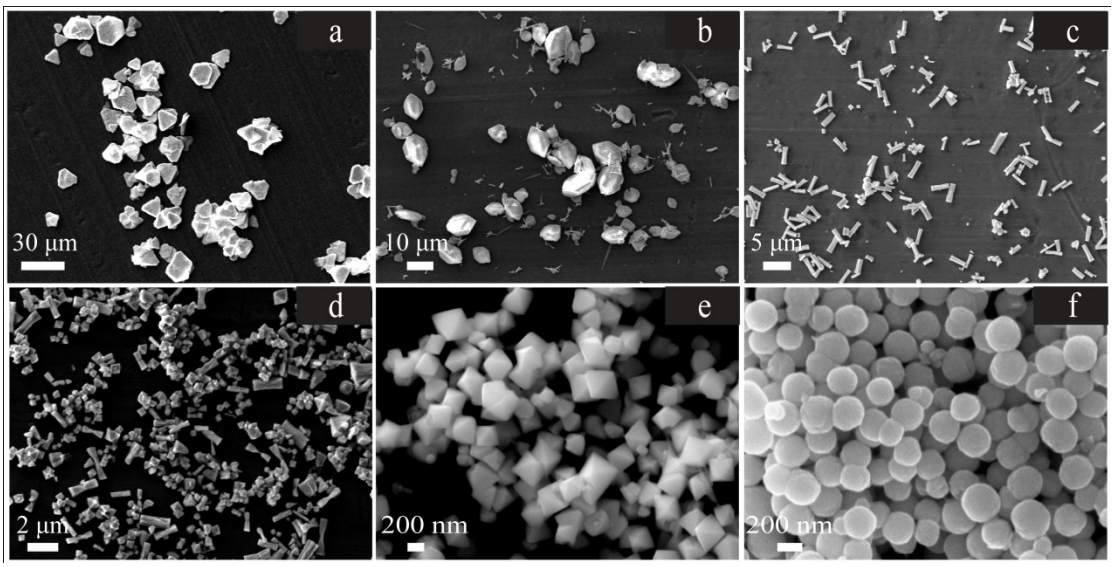

Figure S2. SEM images of products from the experiments described in Table S1. Products: a, $UO_3 \cdot H_2O$; b, $UO_3 \cdot H_2O$ (major) and U_3O_8; c, U_3O_8; d, U_3O_8 (rod) and UO_2 (particle); e, UO_2; f, U_4O_9. XRD patterns for the products are showed in Fig. 1.

The product particle size clearly decreased with the increasing pH values. This reveals that the amount of particles also decreased with the increasing pH values. This is possibly related to the increasing rate of the redox reaction and the degree of supersaturation.

Table S2.1. The experimental parameters for U_3O_8 morphological control.

Sample ID	DI water mL	Acetone mL	UAH mg	$NH_3 \cdot H_2O$ μL	Time h	Morphologies
S2a	7.5	7.5	100	**10**	24	Nail like
S2b	10	10	500	**200**	20	Bone like
S2c	10	5	100	**200**	24	Prism
S2d	7.5	10	200	**50**	20	Spear like
S2e	10	5	200	**100**	20	Bone like

Table S2.2. The experimental parameters for UO_2 morphological control.

Sample ID	DI water mL	Acetone mL	UAH mg	$NH_3 \cdot H_2O$ μL	Time h	Shapes
S2f	5	10	25	**300**	24	Sunk octahedron
S2g	5	10	100	**300**	6	Octahedron
S2h	5	10	100	**400**	6	Sphere & octahedron
S2i	10	10	500	**800**	20	Near sphere

Table S2.1 and S2.2 list the experimental conditions to control the morphology (see Fig. 2) of U_3O_8 (Table S2.1) and UO_2 (Table S2.2), respectively. The results indicate that the higher addition of ammonia (higher pH values) always yield UO_2.

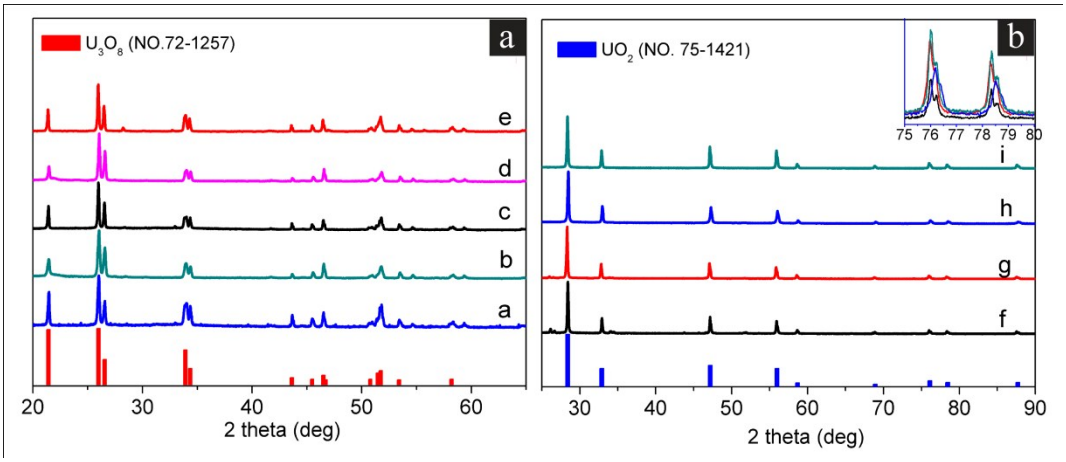

Figure S3. XRD patterns of various morphologies U_3O_8 (a) and UO_2 (b).

XRD patterns indicated U_3O_8 (a) and UO_2 (b) with various morphologies (Fig. 2) obtained at different conditions (Table S2.1 and Table S2.2) are pure phases.

Section 2: multi-monomer growth mechanisms and verified experiments

Table S3.1. The experimental parameters to control compositions (UAH = 200 mg, DI water = 5 mL, acetone = 10 mL, T = 200 °C, t = 6 h).

Sample ID	UAH mg	DI water mL	Acetone mL	$NH_3 \cdot H_2O$ μL	pH	Products
S3-1a	200	5	10	**25**	**5.51**	$U_2(NH_3)\ O_6 3H_2O$
S3-1b	200	5	10	**50**	**7.03**	$U_2(NH_3)\ O_6 3H_2O + U_3O_8$
S3-1c	200	5	10	**75**	**7.56**	$U_2(NH_3)\ O_6 3H_2O + U3O_8$
S3-1d	200	5	10	**100**	**8.13**	$U_3O_8 + UO_2$
S3-1e	200	5	10	**200**	**9.5**	UO_2
S3-1f	200	5	10	**300**	**9.66**	UO_2
S3-1g	200	5	10	**500**	**9.98**	UO_2
S3-1h	200	5	10	**700**	**10.18**	U_4O_9
S3-1i	200	5	10	**800**	**10.28**	U_4O_9
S3-1j	200	5	10	**1000**	**10.42**	U_4O_9
S3-1k	200	5	10	**1500**	**10.51**	U_4O_9

Table S3.2. The experimental parameters to control compositions (UAH=500mg, DI water =10mL, acetone=10mL, T=200,t=20h).

Sample ID	UAH mg	DI water mL	Acetone mL	$NH_3 \cdot H_2O$ μL	pH	Products
S3-2a	500	10	10	**100**	**5.72**	U_3O_8(major) + UO_2
S3-2b	500	10	10	**200**	**6.7**	U_3O_8
S3-2c	500	10	10	**300**	**7.5**	UO_2+U_3O_8
S3-2d	500	10	10	**400**	**8.49**	UO_2+U_3O_8
S3-2e	500	10	10	**500**	**8.86**	U_3O_8 + UO_2(major)
S3-2f	500	10	10	**600**	**9.1**	UO_2

S3-2g	500	10	10	**700**	**9.23**	***UO_2+U_3O_8(major)**
S3-2h	500	10	10	**800**	**9.3**	UO_2
S3-2i	500	10	10	**900**	**9.38**	UO_2
S3-2j	500	10	10	**1000**	**9.45**	UO_2

* The solution was found leaked into AMT7, which lead acetone leakage.

The experiments listed in Tables S3.1and S3.2 exhibited similar results when compared with Table S1despite changing the experimental conditions. The oxidation state of the final products decreased with increasing pH values. The U_4O_9 always appeared after UO_2 and with a shape of sphere, because it formed at a relatively higher reaction rate. Experiments listed in Table S3.1 did not yield pure U_3O_8. The fact that we maintained the precursor (Table S3-1a S3-1b and S3-1c) for 6 hours might explain the increasing concentration of UAH. Experiments did not yield U_4O_9 (Table S3.1) even though the concentration of UAH increased further. The decrease of the MO generation rate could be ascribed by a decrease of the initial acetone concentration.

* The U_3O_8 appeared in the Table S3-2g due to a major acetone leak. This reveals that decreasing the fraction of acetone can reduce system efficiency.

Table S4. The products at varying reaction times (UAH = 100 mg, DI water = 5 mL, acetone = 10mL, ammonia = 300 μ L, T = 200 °C).

Sample ID	DI water mL	Acetone mL	UAH mg	$NH_3 \cdot H_2O$ μL	Time h	Products
S4a	5	10	100	300	**0.5**	**Precursor**
S4b	5	10	100	300	**1**	**Precursor**
S4c	5	10	100	300	**2**	**UO_2+U_3O_8**
S4d	5	10	100	300	**3**	**UO_2+U_3O_8**
S4e	5	10	100	300	**5**	**UO_2+U_3O_8**
S4f	5	10	100	300	**7**	**UO_2**

Note: This experiment cooled rapidly with flowing water, which inhibited the redox reaction and allowed us to retain information on the valence state.

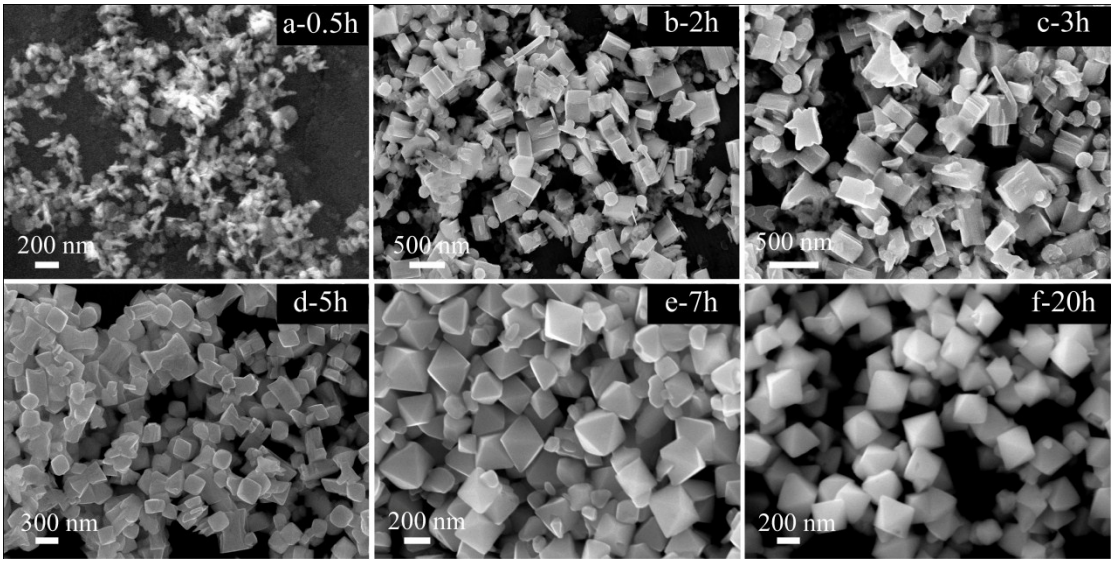

Figure S4. SEM images of products at varying reaction times based on experiments listed in Table S4.

The experiments listed in**TableS4** showed that uranyl (VI) was reduced to U(VI)O_2 with sufficient time. The presence of U_3O_8 indicated that U(VI) and U(V) monomers must exist in the system when the system produces UO_2. This confirms the existence of reduced bi-monomer growth mechanism shown in Fig. 3a. Once the reaction stopped, U_3O_8 could not be removed when we restarted even at long reaction times. This is due to the fact that U_3O_8 is a stable phase and is difficult to dissolve into aqueous. However, $UO_3 \cdot H_2O$ was easy to remove due to its high solubility.

Table S5. The experiments without the addition of ammonia.

Sample ID	UAH mg	DI water mL	Acetone mL	$NH_3 \cdot H_2O$ μL	time h	solid products
S5a	**100**	**5**	**10**	**-**	**6**	**U_3O_8&$UO_3 \cdot H_2O$**
S5b	**100**	**5**	**10**	**-**	**90**	**U_3O_8+UO_2**
S5c	50	5	10	-	90	U_3O_8+UO_2
S5d	200	5	10	-	90	U_3O_8+UO_2
S5e	200	5	10	-	48	U_3O_8+UO_2
S5f	100	10	5	-	48	U_3O_8

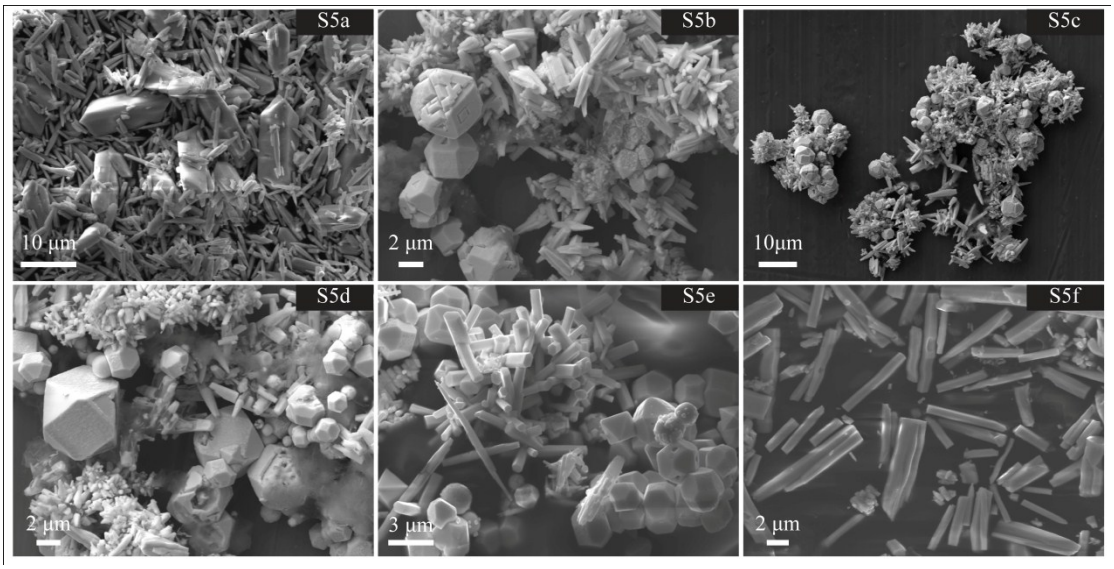

Figure S5. SEM images of products without the addition of ammonia (based on experiments listed in Table S5).

Most products were mixtures that are listed in Table S5 and shown in Figure S5. The system was characterized by efficient reduction, similar to prior experiments, despite no addition of ammonia. This implies that uranium compounds may act as a catalyst to produce MO.

This is different from the experiments listed in Table S4, where $U_3O_8$was still not eliminated after long reaction times (90h) even the experiments were never broke off. This result confirms the mechanism mentioned in Fig. 3b.

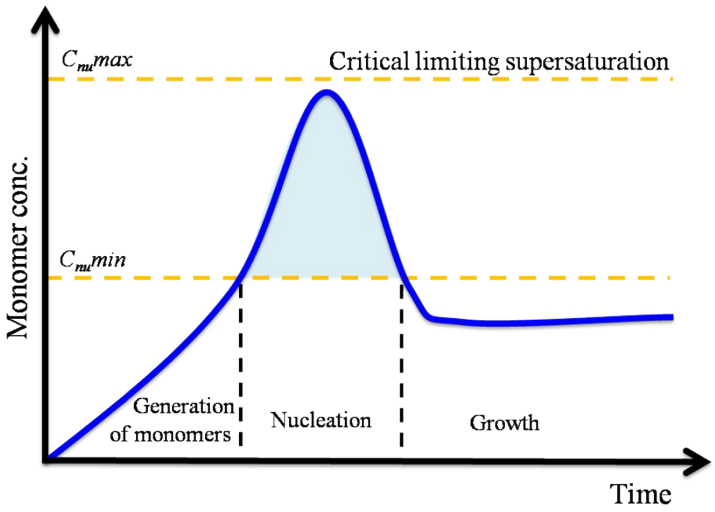

Figure S6. A schematic illustration of the classic LaMer theory. (modified with permission from reference[1], copyright 1950, American Chemical Society).

As described in the LaMer theory, the monomer concentration rapidly increases with time as the precursors reduced or decomposed. As the concentration approaches supersaturation, the monomer begins to aggregate into small clusters or starts self nucleate. Once formed, these nuclei then grow in an accelerated manner and the monomerconcentration drops quickly to below the level of minimum supersaturation. Afterward, no additional nucleationevents occur.

Section 3: Self-catalytic mechanisms and verified experiments

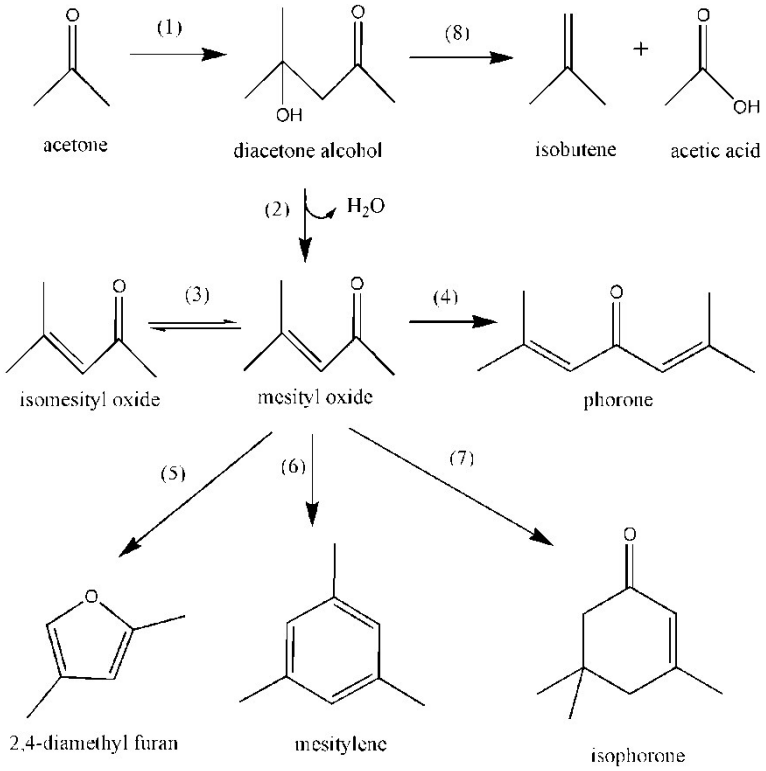

Figure S7. Main reaction pathways for acetone aldolization.[2-7]

Routes (5), (6) and (8) are redox reactions. DAA and MO can potentially act as actual reducing agents. Subsequent GC-MS results showed that the major routes in system are (1), (2), (3), (4), (6) and (7) which implies that MO was the actual reducing agent.

Table S6.1. GC-MS results for the organic products during the acetone reaction at 200 °C (t=20h).

Sample	acetone	UAH	ammonia	organic products（area %）				
ID	mL	Mg	μl	DAA	IMO	MO	Phorone	Isophorone
S6a	15	0	0	97.65%	-	-	-	-
S6b	15	50	0	9.33%	-	22.71%	0.24%	30.75%
S6c	15	50	200	1.70%	0.72%	73.40%	1.35	3.07%

Note:This GC-MS result did not containacetone.

Table S6.2.GC-MS results for the organic products during theMO reaction at 200 °C (t=20h).

Sample	acetone	AA	UAH	Ammonia	organic products（area %）				
ID	mL	mL	mg	μL	Acetone	IMO	MO	Phorone	TMB
S6d	5	10	**50**	-	14.80	3.01	78.62	0.51	1.44
S6e	5	10	**100**	-	11.21	2.77	80.68	0.57	1.83
S6f	0	15	**50**	-	-	3.16	86.58	0.74	**8.01**

GC-MS results listed in **Table S6.1** show that acetone was transferred to DAA without the addition of UAH and ammonia. The aldol reaction is possible with the addition of UAH. The MO fraction was much higher after the addition of both UAH and ammonia. This implies that basic conditions are advantageous to the aldol reaction. The experiments listed in **Table S6.2** verify the MO's ability to reduce and indicated that the oxidation product of MO is trimethylbenzene (TMB).

Table S7. GC-MS results for the organic products at different reaction time.

Sample ID	Reaction time	Solid products	organic products, detected by GC-MS（ % area）				
			acetone	MO	DAA	AA	by-products
S4a	**0.5h**	Precursor	77.66	1.79	13.06	-	7.49
S4b	**1h**	Precursor	77.85	3.16	12.06	-	6.93
S4c	**2h**	UO_2+U_3O_8	80.19	5.04	9.65	-	5.12
S4d	**3h**	UO_2+U_3O_8	82.71	5.36	8.33	-	3.6
S4e	**5h**	UO_2+U_3O_8	81.01	5.07	8.19	-	5.73
S4f	**7h**	UO_2	83.06	3.58	4.45	7.72	1.19
S4a	**20**	UO_2	-	-	-	-	-

Note: Experimental conditions are listed in Table S4.

The GC-MS results listed in **Table S7** reveal that the MO fraction increased with the reaction time after the initial 3 hours. The decrease in the MO fraction later in the experiment may be due to increasing side reactions and subsequent depletion in redox reactions.

Table S8.1. GC-MS results of experiments in Table S8.2.

Sample ID	organic products （% area）					
	acetone	IMO	MO	DAA	acetic acid	by-products
S8a	92.48	-	0.5	2.28	0.47	0
S8b	91.14	-	1.18	7.41	0.26	0.01
S8c	85.36	-	1.97	12.67	√	0
S8d	84.95	-	1.29	13.67	√	0.09
S8e	39.54	√	1.27	24.32	√	**34.87**

Symbol '√' means that this product was detected but the content was low (% area <0.01).

Table S8.2. Experiments to verify the self-catalytic mechanism.

Sample ID	experiments conditions				
	DI water mL	acetone mL	UAH mg	ammonia μL	time h
S8a	5	10	20	**25**	1
S8b	5	10	20	**50**	1
S8c	5	10	20	**100**	1
S8d	5	10	20	**500**	1
S8e	5	10	20	**1000**	1

The GC-MS results listed in Table S8.1 indicate that the MO proportion increased simultaneously with the increasing pH values in the beginning. The proportion of by-products also visibly increased at higher pH values, which is the reason that the MO faction decreased at a higher pH values.

1. Chemicals

Uranyl acetate hydrate (UAH, 99%) was purchased from CAS`MART. Acetone (98%), mesityl oxide (MO, 99%), ammonia, were purchased from Aldrich.

2. Synthesis of uranium oxide nanocrystals

UAH (100mg) was dissolved in a mixture of DI water (5mL) and acetone (10mL) in a capped glass bottle under magnetic stirring. Ammonia range 25μL to 1500μLwas added in the solution to adjusting the pH value. Stirring for 5 minutes after the ammonia was added. The whole mixture was transferred into 30-ml Teflon-lined stainless steel autoclave and sealed. The autoclave was maintained at 200°C for 6 hours and cooled down naturally to room temperature. Solid products were formed at bottom of the autoclave. The precipitates were centrifuged, washed by ethanol and acetone, repeat several times.

Control experiments were carried out by adjusting the hydrothermal temperature, reaction time, concentration of UAH, the volume ratio of acetone to DI water and the volume of $NH_3 \cdot H_2O$, while the other reaction parameters were kept constant. Detailed parameters were showed in the tables.

3. Characterization

The surface morphologies of the powders were observed by field-emission scanning electron microscopy (FE-SEM) using ZIESS SUREA55 microscope. The XRD measurement were performed with a Philip X`Pert Pro diffractometer using Cu Kα radiation at 40kV and 45mA. Gas chromatography mass spectrum (GC-MS) measurement was performed with a SHIMADZU GCMS-QP2010 Plus instrument. The XPS measurement was performed with a Thermo Fisher Scientific ESCALAB 205XI using Al Kα radiation.

Reference

1. V. K. LaMer and R. H. Dinegar, *Journal of the American Chemical Society*, 1950, **72**, 4847-4854.
2. G. Zhang, H. Hattori and K. Tanabe, *Applied Catalysis*, 1988, **36**, 189-197.
3. C. O. Veloso, J. L. F. Monteiro and E. F. Sousa-Aguiar, in *Studies in Surface Science and Catalysis*, eds. J. Weitkamp, H. G. Karge, H. Pfeifer and W. Hölderich, Elsevier, 1994, vol. 84, pp. 1913-1920.
4. W. Xu and D. Raftery, *Journal of Catalysis*, 2001, **204**, 110-117.
5. V. K. Díez, C. R. Apesteguía and J. I. Di Cosimo, *Journal of Catalysis*, 2006, **240**, 235-244.
6. H. Idriss, *Surface Science Reports*, 2010, **65**, 67-109.
7. E. Iglesia, D. G. Barton, J. A. Biscardi, M. J. L. Gines and S. L. Soled, *Catalysis Today*, 1997, **38**, 339-360.